Journal of Alloys and Compounds 1011 (2025) 178471

Contents lists available at ScienceDirect

Journal of Alloys and Compounds

journal homepage: www.elsevier.com/locate/jalcom

MOF-derived nanoceria/graphitic carbon nitride as an efficient electrochemical modifier for guanine sensor with diffusional response

Branka B. Petković [a,*], Hristo Kolev [b], Djordje Veljović [c], Dalibor M. Stanković [d,e], Bratislav Antić [e], Miloš Ognjanović [e,*]

[a] University of Priština in Kosovska Mitrovica, Faculty of Sciences and Mathematics, Lole Ribara 29, Kosovska Mitrovica 38220, Serbia
[b] Institute of Catalysis, Bulgarian Academy of Sciences, Sofia 1113, Bulgaria
[c] Faculty of Technology and Metallurgy, University of Belgrade, Belgrade 11000, Serbia
[d] Faculty of Chemistry, University of Belgrade, Studentski trg 12-16, Beograd 11000, Serbia
[e] "VINČA" Institute of Nuclear Sciences - National Institute of the Republic of Serbia, University of Belgrade, Belgrade, Serbia

ARTICLE INFO

Keywords:
CeBTC
Nanoceria
Carbon paste electrode
Guanine determination
Diffusional response

ABSTRACT

This work presents a novel approach for the electrochemical detection of guanine (GU) using a MOF-derived nanomaterial. CeBTC MOF-derived CeO_2 nanoparticles, prepared by calcination and mixed with graphitic carbon nitride (g-C_3N_4) were structurally and electrochemically characterized and further applied in sensing of GU. XRPD, FTIR, SEM, and XPS measurements were used to study the composition, structure, and morphology of the nanoceria/g-C_3N_4 electrode modifier. Electrochemical impedance spectroscopy measurements and cyclic voltammetric studies indicated an improved electrocatalytic output of nanoceria/g-C_3N_4 modified carbon paste electrode (MOFdCeO_2/g-C_3N_4/CPE). The optimal content of electrode modifier in CPE, experimental conditions, and analytical technique parameters were established to achieve sensitive quantification of GU. Kinetic parameters of the electrochemical reaction of GU were determined and a diffusional response at an electrochemical sensor was achieved. The linear working range of the developed square-wave voltammetric method (SWV) in Britton Robinson buffer solution pH 3.0 at MOFdCeO_2/g-C_3N_4/CPE was recorded from 0.5 μM to 100 μM of GU, with a detection limit of 0.12 μM. The proposed guanine sensor showed good storage stability, repeatability, and selectivity, and its real sample applicability was successfully tested by quantification of guanine in spiked urine samples, with excellent accuracy and precision.

1. Introduction

Metal-organic frameworks (MOFs), the orderly structure of metal nodes in organic linkers, have drawn scientific attention due to their superior material properties. Based on high chemical stability, relatively large specific surface areas, high porosity, and tunable structure, MOFs and MOF-derived materials are found their possible applications in catalysis, batteries, conversion, separation, and gas sensors [1,2]. Functional nanostructures can be easily and successfully prepared by thermolysis of MOFs. Besides conventional methods for synthesizing of metal-oxide nanoparticles [3], they could also be obtained from MOFs. These frameworks represent flexible templates that, through a controlled thermal decomposition process, can produce oxide nanoparticles with even the dispersion of metals on its network. In recent times, various metal oxides like NiO, CeO_2, CuO, Fe_2O_3, Co_3O_4, PdCoOx and others have been obtained in this way and electrochemically applied as energy storage devices [4,5], for catalysis [6,7] and degradation [8], for determining total antioxidant capacity [9] and employed as sensors [10,11].

Guanine, a derivative of purine, is one of the main nucleotide bases found in DNA and RNA. Detecting guanine using electrochemical sensors has gained significant attention due to its role in biological processes [12,13] and as an indicator of oxidative DNA damage [14]. Although GU was electrochemically determined by different methods and modified electrodes [15–26] it is still a challenge to determine low concentrations of this compound, usually present in small amounts in biological complex matrices [27]. Fouling of the electrode surface is another problematic issue, and it is connected with absorption of guanine oxidation products on it. This leads to the decrease in sensitivity and reproducibility of guanine determination over time, affecting the

* Corresponding authors.
E-mail addresses: branka.petkovic@pr.ac.rs (B.B. Petković), miloso@vin.bg.ac.rs (M. Ognjanović).

https://doi.org/10.1016/j.jallcom.2025.178471
Received 23 September 2024; Received in revised form 4 December 2024; Accepted 2 January 2025
Available online 3 January 2025

stability and efficiency of the sensor itself [15]. Electrochemical determination of nanomolar concentrations of guanine was achieved on molecularly imprinted polymer-based electrochemical sensor [16], while recently reported highly sensitive determination of purine bases on ZIF-8-derived hollow N-doped carbon dodecahedron and AuNPs [17] which draw attention on the possibility of successful application of MOF derived nanostructures in composite materials for efficient determining of guanine.

Based on the exceptional catalytic properties of nanoceria (CeO_2 NPs), originating from its potential of reversible switching valence Ce^{3+}/Ce^{4+} [28] we assumed the possibility that MOF derived CeO_2 nanostructures could enhance guanine oxidation signals. CeMOFs can be synthesized with different organic linkers [29], and H_3BTC (benzene-1, 3,5-tricarboxylic acid) based CeMOF (CeBTC) is the most used as a precursor for obtaining nanoceria for catalytic purposes [30].

We have previously studied a combination of metal or metal oxide nanoparticles with carbonaceous materials. They have shown excellent catalytic performance and have been successfully incorporated into electrochemical sensors for the detection of biocompounds [31–34]. Still, in this work, we explored a new approach to develop a nanocomposite modifier by utilizing metal-oxide nanoparticles prepared by thermolysis of the metal-organic framework. We synthesized CeBTC in an aqueous solution at low temperature. Further, we used it as a dispersion precursor for forming porous CeO_2 NPs with uniformly encapsulated cerium ions, controlling the agglomeration. Thermal decomposition was achieved by simple calcination of CeBTC at 450 °C in air, and obtained cerium(IV) oxide particle size was at the nano level and the average crystallite size was about 7 nm. To enhance electrical conductivity and performance, MOF-derived CeO_2 NPs were combined with a two-dimensional graphitic carbon nitride network (g-C_3N_4) to create a highly conductive and efficient modifier for carbon paste electrodes. The kinetic parameters of the electrode process were determined and, a stable diffusion-controlled response was achieved. The developed electrochemical sensor was successfully applied to the quantitative analysis of guanine in spiked human urine samples, demonstrating its reliability and practical utility.

2. Experimental

2.1. Chemicals

Cerium(III)-chloride heptahydrate and benzene-1,3,5-tricarboxylic acid (BTC), used as a linker for the synthesis of CeBTC, were acquired from Alfa Aesar (USA). Urea, guanine hydrochloride, paraffin oil, and glassy carbon powder (for preparing CPE) were all products of Sigma Aldrich company (USA). All other chemicals used for preparing of the electrolyte (Britton-Robinson buffer), electrochemical characterization, preparing samples, and in selectivity study were reagent grade. Ultrapure water was produced from the Millipore Milli Q system.

2.2. Preparation of CeBTC, g-C_3N_4 and MOF derived nanoceria

CeBTC metal-organic framework was synthesized by a slightly modified previously used procedure [35]. The first solution was obtained by mixing 0.25 mmol of $CeCl_3 \bullet 7\ H_2O$ with ultrapure water to obtain a 50 mL solution. In the second solution, 0.25 mmol of benzene-1, 3,5-tricarboxylic acid was dissolved in 50 mL of ethanol/water solution (v/v = 1:1) under vigorous stirring at room temperature. These two solutions were mixed under a continuous stirring for 1.5 h. A white precipitate of CeBTC was collected by centrifugation, washed several times with ethanol/water (v/v, 1:1), and then dried at 60 °C. CeO_2 NPs were derived by calcination of as-prepared CeBTC at a temperature of 450 °C at 10 °C/min and held at the final temperature for 3 h. After that, the products were cooled down to room temperature naturally.

Graphitic carbon nitride (g-C_3N_4) was synthesized through a simple calcination approach placing 5 g of urea in a ceramic crucible with a cover under ambient pressure in air. Then, the closed crucible was heated in a muffle furnace at 550 °C at a 3 °C/min ramp rate for 3 h. The resulting yellow-colored g-C_3N_4 powder was ground with agate mortar and stored for further electrode modifier preparation.

2.3. Methods and Instrumentation

The crystal structures of the synthesized MOF and its corresponding oxide were determined through X-ray powder diffraction (XRPD) analysis. Dried powder samples were examined using a Smart Lab® high-resolution diffractometer (Rigaku, Japan) provided with a CuKα source of radiation (λ = 1.5406 Å) working at 40 kV and 30 mA. Diffraction patterns were measured within the 2θ range of 5–70°.

ATR-FTIR spectroscopy was used to examine the surface chemistry of the prepared MOF and MOF-derived nanoparticles within the mid-infrared region (4000–400 cm^{-1}). A Nicolet iS50 FT-IR spectrometer (Thermo Fisher Scientific, USA) with a Smart iTR ATR accessory was employed for the analysis. Powdered samples were pressed on a diamond crystal plate using a pivot press to ensure the optimum exposure to the infrared beam. Background spectra collected from a clean diamond crystal were subtracted using OMNIC™ Spectra Software.

The morphology of Ce-MOF and MOFdCeO_2/g-C_3N_4 samples was observed by FE-SEM using a MIRA 3 XMU instrument (TESCAN, Brno, Czech Republic), operated at 20 keV, after deposition of a tin gold layer in sputter coater Polaron SC502 (Fisons Instruments, UK).

X-ray photoelectron spectroscopy (XPS) measurements were performed using an ESCALAB MkII electron spectrometer (Thermo Scientific) with a base pressure of 5×10^{-10} mbar in the analysis chamber. A non-monochromated AlKα X-ray source (1486.6 eV) was used with a pass energy of 20 eV to record high-resolution spectra. A pass energy of 20 eV was used for the hemispherical analyzer. The instrumental resolution, measured as the full width at half maximum (FWHM) of the $Ag3d_{5/2}$ photoelectron peak, was approximately 1 eV. The data was analyzed using Casa XPS software (Casa Software Ltd). The measured spectra were processed to remove X-ray satellites and Shirley-type background. [36]. Peak positions and areas were determined by fitting symmetrical Gaussian-Lorentzian curves. The relative concentrations of the different chemical species were calculated by normalizing the peak areas to their corresponding photoionization cross-sections, as determined by Scofield [37].

Autolab 302 N potentiostat/galvanostat and software NOVA 2.0.2 were used for electrochemical measurements. Cyclic voltammetric (CV) and electrochemical impedance spectroscopy (EIS) measurements were done in the presence of a redox test solution of 5 mM $K_3[Fe(CN)]_6/K_4[Fe(CN)]_6$ (1:1) mixture dissolved in 0.1 M KCl. The electrochemical working cell with a three-electrode system was used for experiments. An Ag/AgCl (saturated KCl) was the reference electrode, a Pt-wire was used as a counter electrode and a modified carbon paste electrode was employed as a working electrode. For EIS measurements the frequency was changed from $1 \cdot 10^5$ Hz to $1 \bullet 10^2$ Hz with a signal amplitude of 5 mV at the potential of 0.05 V. The optimal SWV parameters were found by varying pulse amplitude from 10 to 90 mV, frequency from 10 to 90 Hz, and potential step from 2 to 10 mV/s.

2.4. Fabrication of MOFdCeO_2/g-C_3N_4 modified CPE

A binary composite electrode modifier was prepared by mixing MOF-derived nanoceria and graphitic carbon nitride in a ratio of 3:1 in dimethyl formamide, stirred in an ultrasonic bath for 15 min, and allowed to dry at 40 °C. The powder was collected and used as an electrode modifier, which was used as an electrochemical platform in this research was produced by mixing paraffin oil and glassy carbon powder in a mortar, in a ratio of 1:4. Three modified electrodes were prepared using 5 %, 10 %, and 15 % of the modifier relative to the amount of carbon powder. The MOFdCeO_2-CPE and g-C_3N_4-CPE electrodes were prepared using the same procedure. After standing

overnight a portion of the resulting paste was used to fill the carbon paste electrode holder, and the surface was polished using a PTFE plate or wet filter paper before every measurement. The carbon paste was modified by adding a certain percentage (m/m) of the synthesized modifier.

3. Results and discussion

3.1. Material structure and morphology study

The crystal structures of the samples were determined by X-ray powder diffraction (XRPD) patterns are shown in Fig. 1a. Diffraction patterns confirmed the formation of the desired metal-organic framework, Ce-MOF, based on cerium linked to BTC [35]. The thermally decomposed products were also characterized by XRPD. Fig. 1a shows the formation of pure cubic MOF-derived CeO_2 (indexed in Fm-3m, No. 225 crystal phase) with an average crystallite size of approximately 7 nm after the calcination of CeBTC [38]. The average crystallite size was estimated using the Scherrer equation: $B(2\theta) = K\lambda/L{\cdot}\cos\theta$, where $B(2\theta)$ is the peak width at a specific 2θ value, λ is the X-ray wavelength, L is the crystallite size. K is a constant typically assumed to be 1.0 for spherical particles. The Scherrer equation relates the peak broadening in an X-ray diffraction pattern to the crystallite size.

The ATR-FTIR spectra of CeBTC and MOFdCeO$_2$ show peaks between 630 and 760 cm^{-1}, atributed to in-plane and out-of-plane bending vibrations of the aromatic ring (Fig. 1b). The band around 1110 cm^{-1} is assigned to the symmetric and asymmetric C–O stretching vibrations of the carboxylate groups. Strong absorption bands at 1365, 1428, and 1608 cm^{-1} are characteristic of carboxylate group vibrations in mesoporous CeBTC, consistent with the asymmetric, symmetric C═O stretching modes and C–O stretching mode associated with the binding of carboxylate (COOH) groups to Ce ions [39]. Most of these bands, along with the characteristic bands of the COO^- groups of BTC_3^-, are observed in the FTIR spectrum. The band around 486 cm^{-1} is attributed to the O–Ce–O stretching vibration. The vibrations at 3400 cm^{-1} were observed due to the adsorbed water on the surface.

The morphology of Ce-MOF and MOFdCeO$_2$/g-C_3N_4 particles is shown in Fig. 2. Urchin-like agglomerates of a few microns in size, composed of rod-shaped particles, were dominant in both cases at 10,000x magnification (Fig. 2a,d). A certain amount of deagglomerated Ce-MOF particles is also visible at higher magnifications. Ce-MOF rod-shaped nanoparticles were observed at high magnification, confirming the nanostructure of the particles (Fig. 2b, c). In the case of composite MOFdCeO$_2$/g-C_3N_4 powder, two different levels of contrast related to two different morphologies were visible at 50,000 × and 100,000 × magnification. The first morphology is similar to that of Ce-MOF (Fig. 2e), while the second shows a porous graphitic carbon nitride structure with incorporated deagglomerated nanoparticles of CeO_2 (Fig. 2f).

The oxidation states and surface atomic concentrations of the elements present on the surface of the CeO_2 nanoparticle sample were investigated using Electron Spectroscopy for Chemical Analysis, commonly known as X-ray Photoelectron Spectroscopy (XPS). The survey spectra of the light-yellow CeO_2 powder sample, measured using AlKα (blue line) and MgKα (red line) radiation, are presented in Fig. 3a. The XPS data reveal core-level peaks corresponding to cerium (Ce 3d) and oxygen (O 1 s), which constitute the nanoparticles. Additionally, trace amounts of chlorine (Cl 2p core-level) and carbon (C 1 s core-level) from the preparation process are also detected. Further insights can be obtained from the high-resolution XP spectra shown in Fig. 3b, c.

The Ce 3d core-level region is depicted in Fig. 3b. The curve's line shape corresponds to the $3d_{5/2}$ peak with a binding energy of 882.5 eV, accompanied by the $3d_{3/2}$ peak at 898.3 eV, and a satellite peak at a binding energy of 916.9 eV, characteristic for Ce^{4+} oxidation state. Consequently, we attribute the oxidation state of cerium predominantly to Ce^{4+}, consistent with the findings of Maslakov et al. (2018) [40]. However, closer inspection reveals a slight deviation from the standard line shape associated with the Ce^{4+} oxidation state, suggesting that a portion of the cerium on the surface may exist in the reduced Ce^{3+} oxidation state. It is well known that X-ray irradiation can disrupt the bonds between cerium and oxygen, potentially leading to the formation of Ce^{3+}. To mitigate this effect, we performed careful measurements, reducing the exposure time to less than 5 minutes to prevent X-ray-induced reduction while maintaining spectrum quality. By applying the curve-fitting procedure described by Matolín et al. [41], we estimated the ratio of Ce^{3+} to Ce^{4+} on the surface of the CeO_2 nanoparticles to be 0.15. The presence of Ce^{3+} can be attributed to dangling bonds on the nanoparticle surface. The high-resolution XP spectrum of the O 1 s core-level is shown in Fig. 3c. Curve fitting reveals the components of the O 1 s peak, with a peak at 529.4 eV corresponding to Ce-O bonds, as expected, and a peak at 531.0 eV indicating non-lattice oxygen and/or oxygen defects with low coordination. A minor concentration of oxygen bonded to organic species, originating from the nanoparticle preparation process, was also detected at 527.8 eV binding energy. Considering the surface atomic concentrations of total cerium and oxygen, excluding carbon and chlorine contamination, we calculated a Ce/O ratio of 0.43

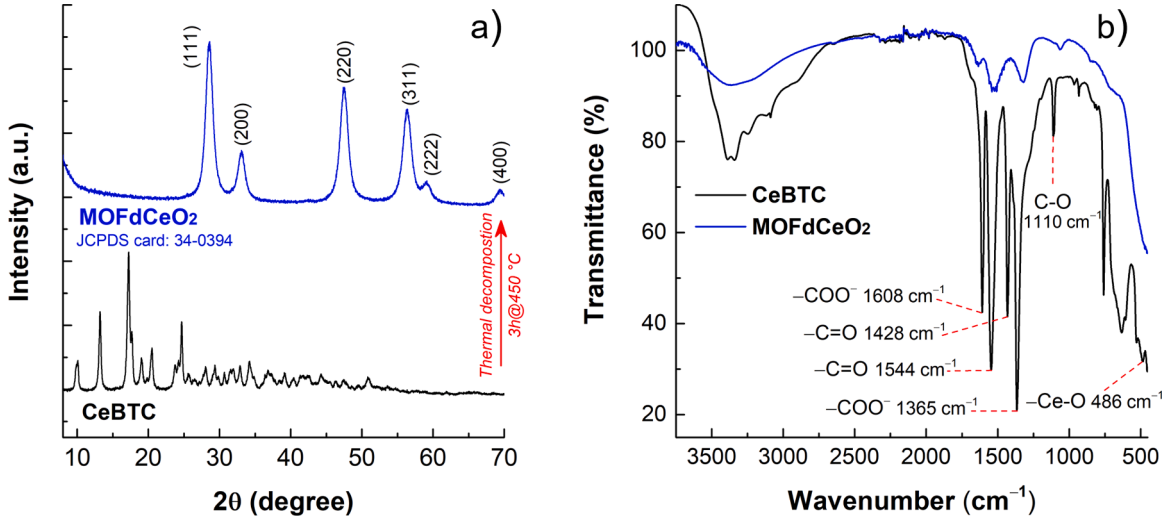

Fig. 1. a) XRPD diffraction patterns of CeBTC (*below*) and MOF-derived cerium oxide after the calcination (above) and b) ATR-FTIR spectra of CeBTC and MOFdCeO$_2$.

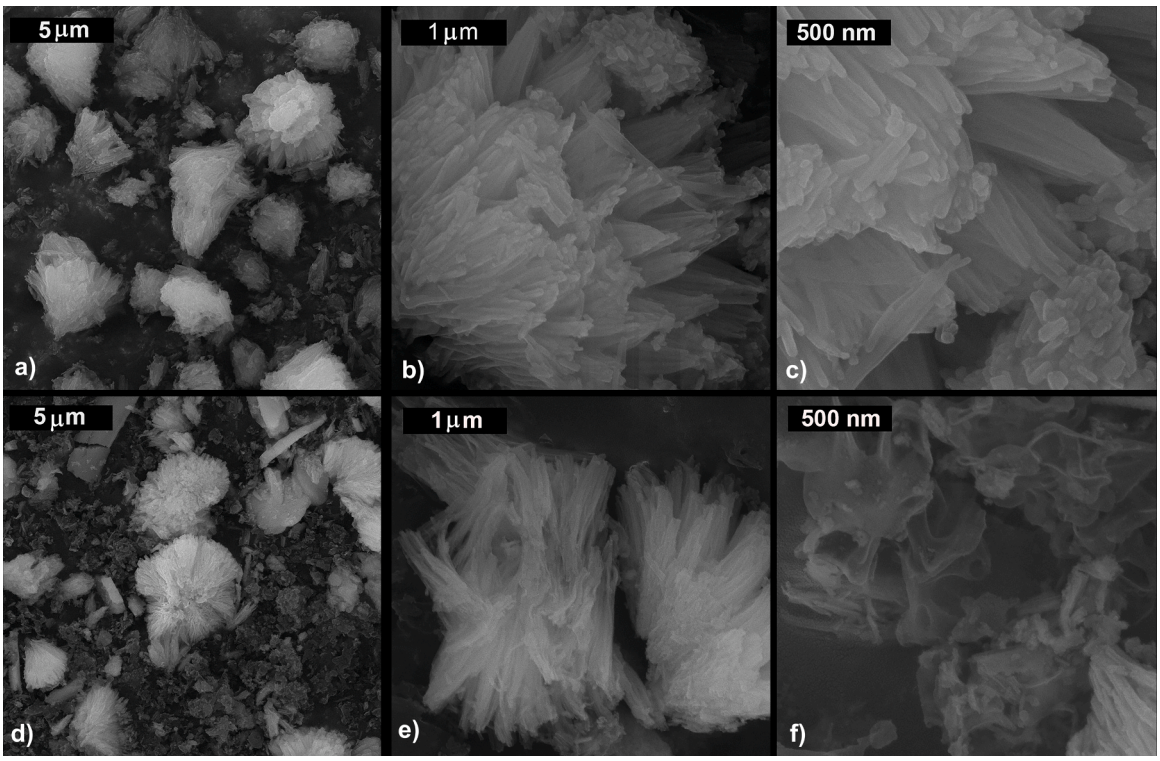

Fig. 2. SEM micrographs of: a,b,c) Ce-MOF; d,e,f) MOFdCeO_2/g-C_3N_4 powders.

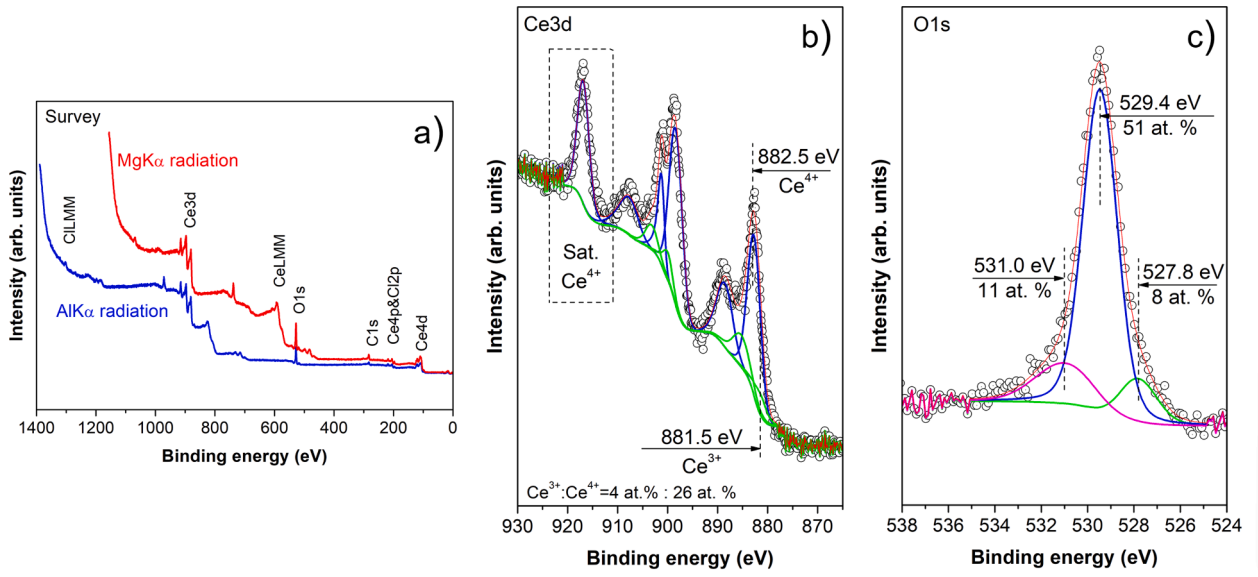

Fig. 3. a) XP survey spectra of CeO_2 powder nanoparticles sample. The blue curve was recorded with AlKα irradiation, while the red curve was recorded with MgKα irradiation. High-resolution XP curve-fitted spectra of CeO_2 nanoparticles: (b) Ce 3d core-level; (c) O 1 s core-level.

from the XPS data. This ratio is close to the theoretical value of 0.5 for CeO_2. The slight discrepancy between the experimental and theoretical ratios is primarily due to the presence of Ce^{3+} on the nanoparticle surface, with additional contributions from standard errors in the XPS experiment. The XPS data and analysis indicate that the CeO_2 nanoparticles possess a minor concentration of reduced Ce^{3+} ions on their surface.

3.2. Electrochemical characterization of electrode material

The combination of CeO_2 nanoparticles and graphite carbon nitride intrigued the researchers and this binary electrode material was investigated before [42,43]. Recently, polyaniline-supported g-C_3N_4/CeO_2 was employed as a chemosensor for selected heavy ions [44]. Pyrolysis decomposed Ce-MOF/g-C_3N_4 was used for sensing dopamine [10] while graphite carbon nitride was doped with MOF-derived CeO_2 to produce photocatalyst for H_2 production [45].

Contrary to the last-mentioned study, in this work, we use CeO_2/g-C_3N_4 composite material as electrode modifier and MOF-derived nanoceria nanoparticles were dominant in its composition. Our previous CV and EIS investigations in $[Fe(CN)_6]^{3-/4-}$ redox system showed that the most conductive electrode modifier was obtained when nanoceria and g-

C_3N_4 were mixed in 3:1, and that ratio was detained in further experiments.

Based on the results of CV and EIS measurements in $[Fe(CN)_6]^{3-/4-}$ test solution, the electrochemical properties of electrode modifiers were explored and the optimal material and its composition were chosen. Comparing the influence of each of the modifiers, it can be concluded that the tested cerium dioxide significantly increases the intensity of the currents (20 %) obtained for both oxidation and reduction processes about the unmodified electrode, confirming its excellent electrocatalytic capabilities. On the other hand, the graphite carbon nitride itself, due to its highly conductive nature, increases the electroactive surface area of the electrode, which results in a decrease in the difference in the potentials (ΔE) of the oxidation and reduction peaks, from $\Delta E_{pristineCPE} = 202$ mV to $\Delta E_{g\text{-}C3N4} = 98$ mV. Finally, their synergetic effect is shown through an increase in current by about 60 % and reduced peak-to-peak separation compared to the unmodified electrode, which shows that the composite has a significant improvement in electrocatalytic ability, which is reflected in a significant increase in diffusion, mass transfer, and charge transfer.

CV profiles in Fig. 4a, b revealed reversible oxidation process at all investigated electrodes, and the reduction to oxidation currents ratio (I_{pa}/I_{pk}) is about 1.00. From Fig. 4a it is evident that the addition of graphite carbon nitride and MOF-derived nanoceria particles separately in CPE enhanced electrochemical response, while the best electrochemical response in $[Fe(CN)_6]^{3-/4-}$ test solution was recorded at CPE modified with their combination. The highest peak current was reached with the optimal amount of 10 % of this binary composite in CPE and from (Fig. 4b) is evident that further addition of the modifier would only significantly decrease the peak current. The same conclusion was revealed from the EIS study recorded in the same test solution. The semicircle at the EIS spectra and following up linear part of the curve can offer information about charge transfer resistance and diffusion process on the electrode surface. In this regard, it can be seen from Fig. 4c and d that the semi-circle region of the modified CPEs was reduced compared to unmodified CPE, which implies that the cerium oxide and graphite carbon nitride, particularly in their optimal amount of 10 % in binary composite, significantly improves the charge transfer reactions which occur at the interface.

3.3. Electrochemical behavior of guanine at $MOFdCeO_2/g\text{-}C_3N_4$ modified electrode

CPE-modified electrode with chosen $MOFdCeO_2/g\text{-}C_3N_4$ binary composite in optimal content was used in further experiments to study the electrochemical behavior of guanine by cyclic voltammetry studies in Britton-Robinson buffer compared with the electrochemical response at pristine CPE and in pH range from 2.0 to 9.0 (Fig. 5). One sharp irreversible anodic peak from guanine oxidation at 0.96 V can be seen in Fig. 5a on both electrodes (modified and pristine CPE) in pH 3.0 at a scan rate of 50 mV/s. Electrooxidation of GU at $MOFdCeO_2/g\text{-}C_3N_4$/CPE is highly promoted by electrode modification and the peak current recorded at the modified electrode is 3.5-fold higher compared to pristine CPE. As can be seen from Fig. 5b, the peak current has been changed and moved towards more positive potentials by increasing pH from 2.0 to 9.0. The relationship between peak potential (E_{pa}) and pH was linear (Fig. 5c) and it can be described by the following Eq. (1):

$$E_{pa}\ (V) = 1.12 - 0.051\ pH;\ (R = 0.9869) \quad (1)$$

The slope of 0.051 V/pH strongly implies that an equal number of protons and electrons are included in the electrode reaction process. pH 3.0 was chosen for the optimal pH value of BR buffer, due to its sharp and well-defined peak shape, the highest current (Fig. 5c). This pH was used in further CV experiments and the development of the analytical procedure.

3.4. Effect of scan rate and the diffusional response

CV profiles on different scan rates and relationships derived from this study can provide important information and kinetic parameters about the electrochemical process at the electrode surface. The effect of scan

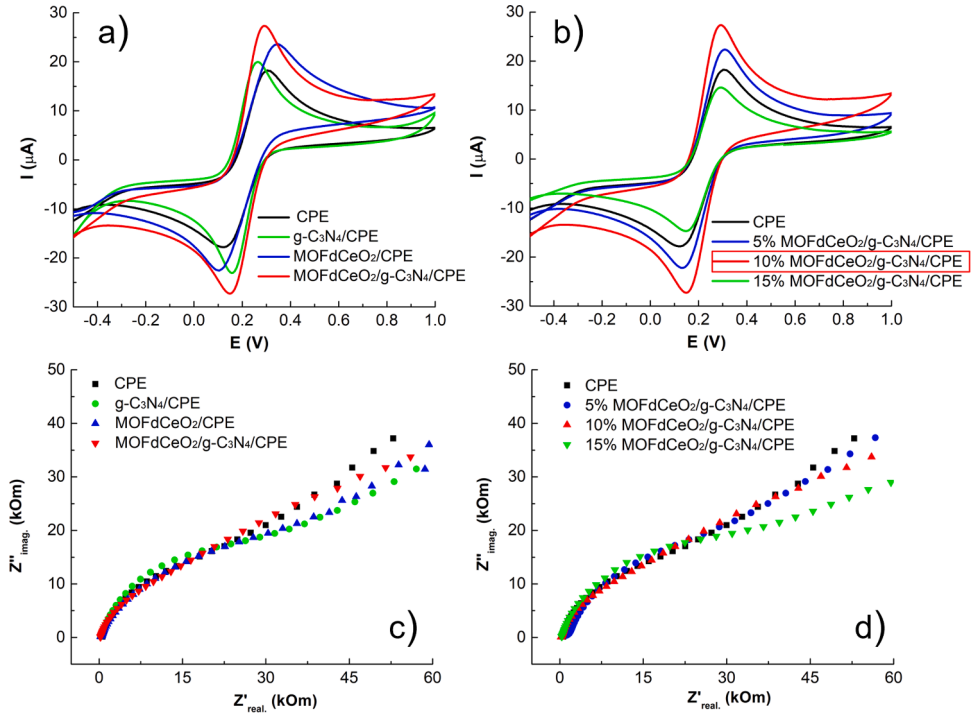

Fig. 4. a) CV profiles of CPE doped with CeO_2 and g-C_3N_4 (pristine and in composite) recorded in 0.1 M KCl solution containing 5 mM $[Fe(CN)_6]^{3-/4-}$ redox couple (scan rate: 50 mV/s); b) CVs of $MOFdCeO_2/g\text{-}C_3N_4$ modified CPEs with different amounts of modifier; c,d) EIS spectra of the investigated electrodes in $[Fe(CN)_6]^{3-/4-}$ solution.

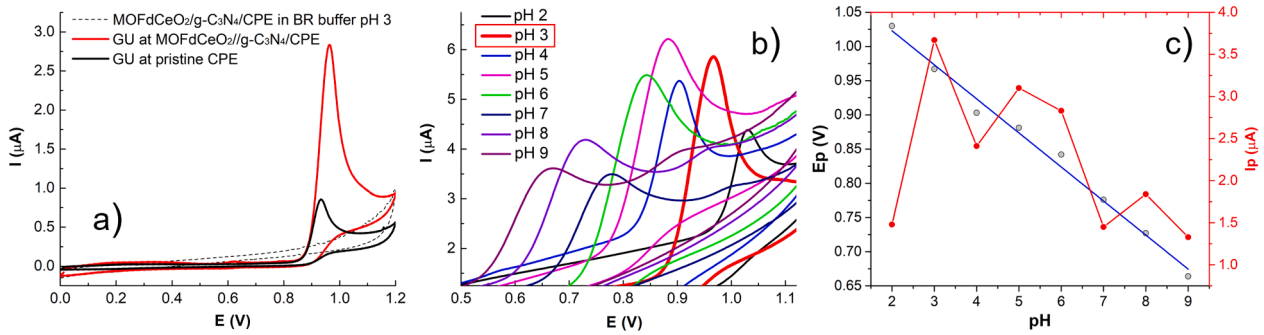

Fig. 5. a) CV profiles with and without 100 μM of GU at MOFdCeO$_2$/g-C$_3$N$_4$/CPE and the same concentration of GU at pristine CPE in BR buffer pH 3.0; b) Effect of pH at MOFdCeO$_2$/g-C$_3$N$_4$/CPE. The scan rate of 100 mV/s; c) The effect of pH of BR buffer on peak current and peak potential.

rate (in this study: 10, 25, 50, 75, 100, 125 and 150 mV/s) was presented in Fig. 6a. The linear relationships between peak current *vs* square root (Fig. 6a, inset graph above) and the logarithm of peak current *vs* logarithm of scan rate (Fig. 6a, inset graph below) imply that reaction on the MOFdCeO$_2$/g-C$_3$N$_4$/CPE is controlled by diffusion on a rate-determining step while the adsorption and/or other specific interactions on the electrode surface are negligible. The following equations were derived from the obtained results by linear regression fitting (Eqs. 2 and 3):

$$I\,(\mathrm{A}) = -9.86\times 10^{-7} + 5.97\times 10^{-7} \times v^{1/2}\,(\mathrm{mV/s})^{1/2};\ (\mathrm{R} = 0.990) \quad (2)$$

$$\log I\,(\mathrm{A}) = -6.61 + 0.62 \times \log v\,(\mathrm{V/s});\ (\mathrm{R} = 0.998) \quad (3)$$

As can be seen, log *I* vs log *v* resulted in a straight line with a slope of 0.62 and this value is close to the theoretical value of 0.5 which once again suggested the diffusion-controlled process [46].

Tafel plot derived from the rising part of CV recorded at a scan rate of 25 mV/s (Fig. 6b and inset plot) corresponded to the linear regression Eq. (4):

$$E\,(\mathrm{V}) = 0.071\ \log I\,(\mathrm{A}) + 0.1347;(\mathrm{R} = 0.997) \quad (4)$$

The Tafel plot slope of 71 mV is close to the theoretical value of 60 mV, indicating that two electrons were involved in charge transfer in the electrooxidation process of GU at MOFdCeO$_2$/g-C$_3$N$_4$/CPE. The small slope of the Tafel plot suggested a fast electron transfer with minimal kinetic barriers. Diffusion-controlled process at electrode interface ensures sustained reaction rate, better quantitative detection, fouling resistance and stabile and reversible sensor response. Diffusion-controlled sensors where the analyte is consistently available at the electrode surface and continuously replenishes itself from the bulk solution making it that concentration gradients drive the reaction are ideal for detecting analytes like guanine in biological samples [47,48]. From Tafel slope electron transfer coefficient α can also be obtained. This slope equals to $2.3RT/Fn(1\text{-}\alpha)$, where *R* and *F* are the Gas and Faraday constant, *T* is absolute temperature, *n* is the number of electrons involved (in this case two) and α was calculated to be 0.58. The standard heterogeneous rate constant of the reaction, k^0, was calculated from Laviron's Eq. (5) for the irreversible electrode process. k^0 has a value of $2.86 \times 10^3\ \mathrm{s}^{-1}$, suggesting fast electron transfer between GU and MOFdCeO$_2$/g-C$_3$N$_4$/CPE surface. (The formal potential, E^0, is 0.9381 V and was obtained from the intercept of Ep *vs* v by extrapolation to the vertical axis to v = 0 mV/s.)

$$Ep = \mathrm{E}^0 + \left(\frac{2.303\mathrm{RT}}{\alpha \mathrm{nF}}\right)\log\left(\frac{\mathrm{RTk}^0}{\alpha \mathrm{nF}}\right) + \left(\frac{2.303\mathrm{RT}}{\alpha \mathrm{nF}}\right)\log v \quad (5)$$

Eqs. (1) and (4) in summary suggested electrooxidation of GU at MOFdCeO$_2$/g-C$_3$N$_4$/CPE, in correlation with previously ascribed in

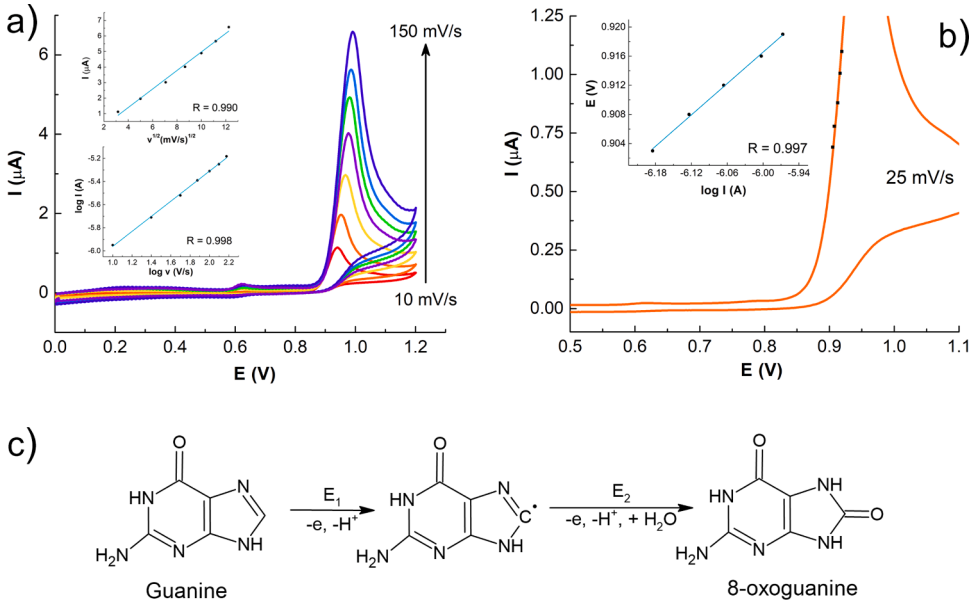

Fig. 6. a) Effect of scan rate (10, 25, 50, 75, 100, 125, 150 mV/s) on CV profiles of 100 μM of GU at MOFdCeO$_2$/g-C$_3$N$_4$/CPE in BR buffer pH 3.0; (inset graph above-plot of peak current *vs* square root of scan rate; inset graph below-plot of log peak current *vs* log scan rate). b) CV of GU at a scan rate of 25 mV/s and chosen data for construction of Tafel plot (inset graph-Tafel plot derived from graph b); c) Suggested mechanism of electrooxidation of guanine.

literature [49–51]. The first oxidation $-2e^-$, $-2H^+$ occurred during the reported complex mechanism, including two-electron transfer processes: E_1, followed by a chemical step, and E_2 to form 8-oxoguanine (peak visible in this study) (Fig. 6c), and then 8-oxoguanine can further undergo reversible $-2e^-$, $-2H^+$ oxidation and rapidly hydrolyze [52].

Bearing in mind previously reported conclusions [52], probably the high influence of the chemical step upon the E2, as a rate-determining step during the all used scan rates from 10 to 150 mV/s existed at MOFdCeO_2/g-C_3N_4/CPE. This diffusional response of GU at the electrode is not highly driven in nature, and it is difficult to achieve on carbon electrodes and modified electrodes. Almost all of the reported GU sensors showed a typical surface absorption-controlled process [15, 17–23,52], even those that have CeO_2 in their constitution [20,21]. This absorption-prone behavior was investigated by tailoring different carbon electrode materials and explained due to the high domination of absorbed species during the electrooxidation of GU at carbon materials [52]. This absorption could be blocked by special pretreatment of the surface during the preparation of the electrode (by cleaning with acetone for example) [52], or using some electrode modifiers more resistant to absorption, as was the case with MOFdCeO_2/g-C_3N_4, used as electrode modifier in this study. The binary composition of electrode modifier with dominant CeO_2 over carbonaceous material g-C_3N_4 could be crucial for the achievement of diffusional response in the CPE matrix, bearing in mind that unmodified CPE also showed diffusional response [53]. The diffusion-controlled process was also achieved before, by modification of GCE with gold-platinum nanoclusters/reduced graphene oxide [24] and Cu−CeO_2 coated multiwall carbon nanotube composite [25].

3.5. Development of the analytical procedure

From an analytical point of view, the diffusion-controlled process of electrochemical reaction at the surface of the electrode is more desirable than surface absorption due to faster response times, improved sensitivity, reduced interference, wider dynamic range, and better overall reproducibility of sensor measurements. After the characterization of the electrode process and obtaining kinetic parameters, an analytical procedure and method are developed.

Primarily, an analytical technique was chosen comparing the electrochemical responses of two of the most used pulse techniques, square-wave and differential pulse voltammetry without optimization and under operating conditions suggested by the equipment manufacturer. As can be seen from this the Fig. 7a, the peak potential for SWV is twice higher than that recorded by the DPV technique. The advantage is also that SWV is much faster than DPV. This method is usually used for the determination of analytes in which the charge transfer is very fast, the better results obtained with this method additionally confirm the fast transfer of electrons over the electrode surface, highlight the diffusion-controlled nature of the electrochemical reaction and the excellent performance of the selected material. Due to higher and more pronounced peak currents, the square-wave voltammetry was chosen. From our research experience, SWV was proved to be a better technique compared to DPV for quantification of analytes (dopamine and lipoic acid), although they have irreversible peaks [31,42], while caffeic acid which possess reversible peaks was better determined with DPV than SWV [33]. The parameters of the technique were systematically varied and optimal ones were established: the pulse amplitude was 50 mV, the frequency was 70 Hz, and the potential step was 5 mV. Under optimal conditions, SWV profiles of different concentrations of GU (0, 0.5, 1, 3, 5, 7, 10, 20, 30, 40, 60, 70, 80, 90, and 100 μM) at MOFdCeO_2/g-C_3N_4/CPE were recorded in BR buffer pH 3.0 (Fig. 7b) and corresponded calibration curve which expressed concentration dependence of peak current was presented at Fig. 7c. The linear relationship for the working range of 0.5–100 μM of GU was described by Eq. 6:

$$I\ (\mu A) = 4.410 + 0.105 \times C_{GU}\ (\mu M);\ (R = 0.997) \quad (6)$$

The detection limit of 0.12 μM was calculated from the equation $LOD = 3\ s/m$, where s is the standard deviation of the blank solution and, m is the slope of the calibration curve. As can be seen from Table 1, the proposed GU sensor has some of the widest working ranges, along with $NpNiMn_2O_4$ modified graphite paste electrode [15], electrochemically modified CPE [24,26], and activated glassy carbon electrode with ultrafine carbide nanocrystals confined within porous nitrogen-doped carbon dodecahedrons (PNCD) synthesized by adding molybdate to ZIF-8 followed by annealing [17]. MOFdCeO_2/g-C_3N_4/CPE is comparable and even possesses better LOD than other reported GU sensors, especially comparing reported chemically and electrochemically modified carbon paste electrodes [18,22,23,26] (except for In–CeO_2/GCPE, which is more suitable for determining lower concentrations of GU

Table 1
Comparison GU electrochemical sensors in analytical parameters.

Electrochemical sensor	Linear range (μM)	LOD (μM)	Ref.
$NpNiMn_2O_4$/GP	0.5–100	0.3	[15]
PPyox/MWNTs-MoS_2/GCE	5–30	0.17	[19]
CeO_2/MWCNTs/GCE	5–50	0.01	[20]
In-CeO_2/GCPE	0.07–34	0.0119	[21]
FeOMCPE	10–70	5.3	[18]
MgO-MWCNTs-MCPE		0.92	[22]
CuO NPsMCPE	1–80	0.687	[23]
AuPtNCs-modified GCE	1–200	0.06	[24]
Cu-CeO_2/MWCNT/GCE	0.2–6	0.128	[25]
GU-MIP-AuSPE	0.05–0.5	0.00125	[16]
AuNPs/MC-PNCDs/AGCE	0.5–160	0.0721	[17]
Electrochemically modified CPE	3.31–331.1 (0.5–50 μg/mL of GU)*	0.331 (50 ng/mL of GU)*	[26]
MOFdCeO_2/g-C_3N_4/CPE	0.5–100	0.12	*This work*

* Original data in the article.

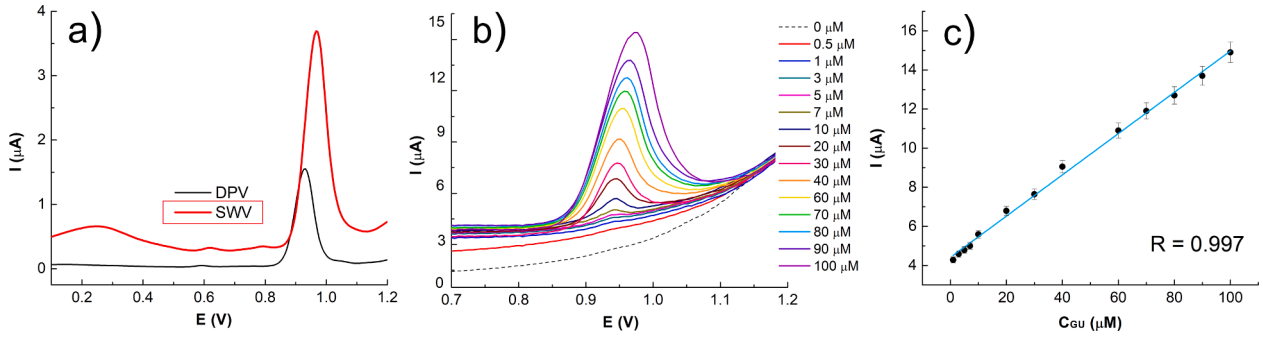

Fig. 7. a) A comparison of GU responses differential pulse voltammetry (DPV) and square wave voltammetry (SWV). b) SWVs for different micromolar concentrations of GU at MOFdCeO_2/g-C_3N_4/CPE in BR buffer pH 3.0. c) Corresponded calibration curve.

[21]). This comparison confirmed the high analytical performance of MOFdCeO$_2$/g-C$_3$N$_4$-modified CPE and developed an analytical procedure for determining guanine.

3.6. Stability study, interferences and real sample analysis

The stability of the prepared modified electrode was studied to investigate reproducibility and long-term applicability. Fig. 8a shows the relative error of five consecutive SWV measurements of 7 μM of GU, taking the initial one as a comparison for the others. The relative standard deviation for those five times repeated measurements of GU at the selected pH and optimal experimental conditions was found to be 1.6 %, and the electrode retained 94 % of the peak current response for initial peak current after 15 days of storing in the ambient conditions after use.

A selectivity study for guanine determination was done in the presence of various inorganic ions and biological compounds. The developed sensor exhibited satisfactory anti-interference ability as the addition of 100 μM of fructose, glucose, lactose, sucrose, citric acid, folic acid, Mg^{2+}, Na^{+}, Ca^{2+}, Al^{3+}, NH_4^{+}, F^{-}, Cl^{-}, SO_4^{2-}, and NO_3^{-} led to a relative error of less than ± 5.0 % in guanine response. The effect of possible interfering ingredients that could be ordinarily found in urine sample was also examined (Fig. 8**b**). Dopamine (DOP) and ascorbic acid (AA) were added in 5:1 ratio to 10 μM of guanine, while uric acid (UA) was added in ratio 0.05:1, because proposed sensor showed high sensitivity toward UA. From the graph, it can be seen that for the addition of AA no peak occurred, the addition of UA significantly reduces dopamine-derived signal, but the GU response remains almost unchanged. Finally, 5 mL of urine was added to 20 mL of the studied solvent with all compounds on it, and the same influence over DOP was observed. The change of peak current for GU determination was less than 5 %, in all cases, showing the high tolerance towards the studied potential interfering biomolecules and indicating the successful real sample determination in the presence of all these compounds.

Bearing in mind previously obtained results of good analytical performances, stability, reproducibility, and selectivity, the MOFdCeO$_2$/g-C$_3$N$_4$/CPE was finally confirmed by sensor applicability in real sample analysis. Before testing, the collected urine samples were acidified for preservation and storied in the refrigerator at 4 °C. 1 mL of urine was added in 20 mL of BR buffer solution pH 3.0 and this solution was spiked with different amounts of guanine for testing of the prepared electrode and developed electrochemical method. The concentrations of the GU were determined from the calibration curve used for determining GU concentration in spiked urine sample (Fig. 7c), and these results and recovery values are listed in Table 2. The proposed method possesses satisfactory accuracy with no/or negligible matrix effect, particularly due to the high oxidation potential of GU at this electrode. Hence, the proposed sensor and developed analytical method were validated in the accurate determining of guanine and further is ready to be used in real sample analysis. Although our proposed sensor was successfully applied for the determination of guanine in model urine samples, it is possible that the determination of this compound would be faced with significant challenges in complex samples like blood and saliva. The problem can be a complex sample composition in which proteins and lipids can be absorbed on the surface of the electrode and interfere the signal. Sample viscosity could also affect sensor performances Bearing all that in mind, it is possible that analysis of complex biological samples like blood and saliva can request sample pretreatment or standard addition procedure and recording calibration curve for GU in matrix.

Table 2
Recovery data for guanine determination was observed for spiked human urine samples.

Sample No	Detected* (μM)	Added * (μM)	Found* (μM)	Recovery (%)
1.	0.00	7.00	6.87 ± 0.04	98.1
	6.87 ± 0.04	3.00	10.32 ± 0.36	103.2
	10.32 ± 0.36	3.00	13.45 ± 0.28	103.5
2.	0.00	20.00	19.66 ± 0.45	98.3
	19.66 ± 0.45	4.00	24.22 ± 0.18	100.9
	24.22 ± 0.18	4.00	28.48 ± 0.42	101.7

[a] An average of three replicate measurements ± SD

4. Conclusion

Obtained results in this research confirmed that cost-effective, easily prepared, BTC-derived nanoceria/graphitic carbon nitride, could be used as an efficient electrochemical sensor modifier for fast, sensitive, and selective guanine determination in test solutions and model urine samples. This binary composite with dominant nanoceria possesses a cubic structure, with an average crystallite size of 7 nm and as a modifier, embedded in carbon paste matrix, provides a fast and stable diffusional response which contributes to analytical performances (wide working range and low detection limit) of developed electrochemical guanine sensor. Our further work will focus on lowering the limit of detection, achieving a diffusional-controlled reaction on a slightly structurally improved combination of MOF-derived nanoceria and carbonaceous materials and exploring the possibility of application of this and mentioned sensors in complex biological samples like blood and saliva with minimal sample preparation required. Based on this one and similar works, the great potential of producing metal oxide nanoparticles and metal/carbon structures from MOF precursors could be observed. Fabrication of MOF-derived materials in combination with conductive carbon materials and networks could be a successful pathway for designing various functional materials with favorable sensor performances toward bioactive compounds.

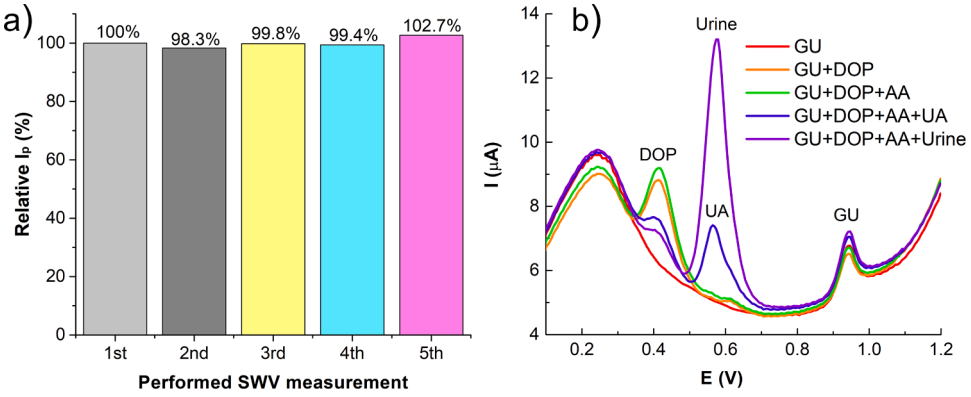

Fig. 8. a) The change in current densities for five consecutive SWV measurements; b) SWV profiles with and without the presence of interfering compounds in the determination of guanine under optimized experimental conditions.

CRediT authorship contribution statement

Branka B. Petković: Writing – original draft, Methodology, Investigation, Formal analysis. **Hristo Kolev:** Writing – review & editing, Validation, Software, Investigation. **Bratislav Antić:** Supervision, Resources, Project administration. **Miloš Ognjanović:** Writing – review & editing, Validation, Resources, Methodology, Investigation. **Djordje Veljović:** Validation, Software, Investigation, Formal analysis, Conceptualization. **Dalibor M. Stanković:** Writing – review & editing, Supervision, Project administration, Methodology.

Declaration of Competing Interest

The authors declare that they have no known competing financial interests or personal relationships that could have appeared to influence the work reported in this paper.

Acknowledgments

Financial support for this study was granted by the Ministry of Science, Technological Development and Innovation of Republic of Serbia Grant No. 451-03-65/2024-03/200123 and 451-03-66/2024-03/200168, the Faculty of Sciences and Mathematics, University of Priština in Kosovska Mitrovica, Project Number IJ-2301 and Bulgarian National Science Found in the frame of the project "Self-heating magnetic nanoconstructs for theranostic applications (Acronym: SeNaTa)", part of "Multilateral scientific and technological cooperation in the Danube region" with numbers No. КП-06-Дунав/4. The research was also funded by the European Union, MOBILES (Monitoring and detection of biotic and abiotic pollutants by electronic, plants and microorganisms based sensors), Grant Agreement 101135402, https://doi.org/10.3030/101135402.

Data availability

No data was used for the research described in the article.

References

[1] D. Li, A. Yadav, H. Zhou, K. Roy, P. Thanasekaran, C. Lee, Advances and applications of metal-organic frameworks (MOFs) in emerging technologies: a comprehensive review, Glob. Chall. (2023) 2300244, https://doi.org/10.1002/gch2.202300244.
[2] L.E. Kreno, K. Leong, O.K. Farha, M. Allendorf, R.P. Van Duyne, J.T. Hupp, Metal–organic framework materials as chemical sensors, Chem. Rev. 112 (2012) 1105–1125, https://doi.org/10.1021/cr200324t.
[3] A.M. Negrescu, M.S. Killian, S.N.V. Raghu, P. Schmuki, A. Mazare, A. Cimpean, Metal oxide nanoparticles: review of synthesis, characterization and biological effects, JFB 13 (2022) 274, https://doi.org/10.3390/jfb13040274.
[4] T. Chen, X. Liu, L. Niu, Y. Gong, C. Li, S. Xu, L. Pan, Recent progress on metal–organic framework-derived materials for sodium-ion battery anodes, Inorg. Chem. Front. 7 (2020) 567–582, https://doi.org/10.1039/C9QI01268K.
[5] X.-C. Xie, K.-J. Huang, X. Wu, Metal–organic framework derived hollow materials for electrochemical energy storage, J. Mater. Chem. A 6 (2018) 6754–6771, https://doi.org/10.1039/C8TA00612A.
[6] Z. Guo, L. Song, T. Xu, D. Gao, C. Li, X. Hu, G. Chen, CeO_2-CuO bimetal oxides derived from Ce-based MOF and their difference in catalytic activities for CO oxidation, Mater. Chem. Phys. 226 (2019) 338–343, https://doi.org/10.1016/j.matchemphys.2019.01.057.
[7] S. Zhang, H. Gao, X. Xu, R. Cao, H. Yang, X. Xu, J. Li, MOF-derived CoN/N-C@SiO_2 yolk-shell nanoreactor with dual active sites for highly efficient catalytic advanced oxidation processes, Chem. Eng. J. 381 (2020) 122670, https://doi.org/10.1016/j.cej.2019.122670.
[8] R. Liang, Z. He, C. Zhou, G. Yan, L. Wu, MOF-derived porous Fe_2O_3 nanoparticles coupled with CdS quantum dots for degradation of bisphenol A under visible light irradiation, Nanomaterials 10 (2020) 1701, https://doi.org/10.3390/nano10091701.
[9] L. Wang, Y. Wang, Y. Zhou, Bimetallic MOF-derived three-dimensional nanoflowers PdCoOx as peroxidase mimic activity for determining total antioxidant capacity, Food Chem. 457 (2024) 140120, https://doi.org/10.1016/j.foodchem.2024.140120.
[10] C. Ge, R. Ramachandran, F. Wang, CeO_2-based two-dimensional layered nanocomposites derived from a metal–organic framework for selective electrochemical dopamine sensors, Sensors 20 (2020) 4880, https://doi.org/10.3390/s20174880.
[11] A.D. Ambaye, T.G. Kebede, B. Ntsendwana, E.N. Nxumalo, Fe-MOF derived graphitic carbon nitride nanocomposites as novel electrode materials for the electrochemical sensing of 2,4-dichlorophenol in wastewater, Synth. Met. 299 (2023) 117452, https://doi.org/10.1016/j.synthmet.2023.117452.
[12] A.L. Burgueño, R. Cabrerizo, N. Gonzales Mansilla, S. Sookoian, C.J. Pirola, Maternal high-fat intake during pregnancy programs metabolic-syndrome-related phenotypes through liver mitochondrial DNA copy number and transcriptional activity of liver PPARGC1A, J. Nutr. Biochem. 24 (2013) 6–13, https://doi.org/10.1016/j.jnutbio.2011.12.008.
[13] J. Wang, Electrochemical nucleic acid biosensors, Anal. Chim. Acta 469 (2002) 63–71, https://doi.org/10.1016/S0003-2670(01)01399-X.
[14] V.C. Diculescu, A.-M.C. Paquim, A.M.O. Brett, Electrochemical DNA sensors for detection of DNA damage, Sensors 5 (2005) 377–393, https://doi.org/10.3390/s5060377.
[15] Electrochemical Sensing of Uric Acid and Guanine Using a Graphite Paste Electrode of NiMn2O4 Spinel Nanoparticles, Biointerface Res Appl Chem 13 (2022) 134. https://doi.org/10.33263/BRIAC132.134.
[16] A. Zolfaghari Asl, A.A. Rafati, S. Khazalpour, Highly sensitive molecularly imprinted polymer-based electrochemical sensor for voltammetric determination of Adenine and Guanine in real samples using gold screen-printed electrode, J. Mol. Liq. 369 (2023) 120942, https://doi.org/10.1016/j.molliq.2022.120942.
[17] H. Lai, Y. Niu, P. Ming, J. Wang, S. Wang, Y. Xu, H. Zhai, An electrochemical sensor for purine base detection with ZIF-8-derived hollow N-doped carbon dodecahedron and AuNPs as electrocatalysts, Anal. Bioanal. Chem. 415 (2023) 855–865, https://doi.org/10.1007/s00216-022-04478-6.
[18] M. S, B.E.K. Swamy, K.A. Vishnumurthy, Iron oxide modified carbon paste electrode sensor for guanine and dopamine: a voltammetric technique, Anal. Bioanal. Electrochem. 15 (2023), https://doi.org/10.22034/abec.2023.705725.
[19] X. Geng, J. Bao, T. Huang, X. Wang, C. Hou, J. Hou, M. Samalo, M. Yang, D. Huo, Electrochemical sensor for the simultaneous detection of guanine and adenine based on a PPyox/MWNTs-MoS_2 modified electrode, J. Electrochem. Soc. 166 (2019) B498–B504, https://doi.org/10.1149/2.1221906jes.
[20] Y. Wei, Q.-A. Huang, M.-G. Li, X.-J. Huang, B. Fang, L. Wang, CeO_2 nanoparticles decorated multi-walled carbon nanotubes for electrochemical determination of guanine and adenine, Electrochim. Acta 56 (2011) 8571–8575, https://doi.org/10.1016/j.electacta.2011.07.048.
[21] H. Ibrahim, Y. Temerk, N. Farhan, Electrochemical sensor for individual and simultaneous determination of guanine and adenine in biological fluids and in DNA based on a nano-In–ceria modified glassy carbon paste electrode, RSC Adv. 6 (2016) 90220–90231, https://doi.org/10.1039/C6RA13704K.
[22] K. Chetankumar, B.E.K. Swamy, H.S.B. Naik, MgO and MWCNTs amplified electrochemical sensor for guanine, adenine and epinephrine, Mater. Chem. Phys. 267 (2021) 124610, https://doi.org/10.1016/j.matchemphys.2021.124610.
[23] S. Ks, B. M, N. K.S, Fabrication of copper oxide nanoparticles modified carbon paste electrode and its application in simultaneous electroanalysis of guanine, adenine and thymine, Sens. Actuators A: Phys. 280 (2018) 277–286, https://doi.org/10.1016/j.sna.2018.07.049.
[24] B. Mao, L. Qian, M. Govindhan, Z. Liu, A. Chen, Simultaneous electrochemical detection of guanine and adenine using reduced graphene oxide decorated with AuPt nanoclusters, Microchim Acta 188 (2021) 276, https://doi.org/10.1007/s00604-021-04926-7.
[25] M. Aktürk, U. Karabiberoğlu, Z. Dursun, Fabrication of Cu−CeO_2 coated multiwall carbon nanotube composite electrode for simultaneous determination of guanine and adenine, Electroanalysis 30 (2018) 238–249, https://doi.org/10.1002/elan.201700590.
[26] A.-N. Kawde, T.A. Saleh, Electrochemical investigation of glassy carbon paste electrode and its application for guanine and ssDNA detection, Chem. Sens 1 (2011) 18–24.
[27] A. Weimann, Quantification of 8-oxo-guanine and guanine as the nucleobase, nucleoside and deoxynucleoside forms in human urine by high-performance liquid chromatography-electrospray tandem mass spectrometry, Nucleic Acids Res. 30 (2002) 7e–77e, https://doi.org/10.1093/nar/30.2.e7.
[28] T. Wang, Y. Hu, M. Liang, L. Song, T. Li, X. Zhang, N. Li, X. Huang, Synthesis of a cerium-based nanomaterial with superior oxidase-like activity for colorimetric determination of glutathione in food samples, Microchim Acta 189 (2022) 132, https://doi.org/10.1007/s00604-022-05197-6.
[29] J. Jacobsen, A. Ienco, R. D'Amato, F. Costantino, N. Stock, The chemistry of Ce-based metal–organic frameworks, Dalton Trans. 49 (2020) 16551–16586, https://doi.org/10.1039/D0DT02813D.
[30] T. Montini, M. Melchionna, M. Monai, P. Fornasiero, Fundamentals and catalytic applications of CeO_2-based materials, Chem. Rev. 116 (2016) 5987–6041, https://doi.org/10.1021/acs.chemrev.5b00603.
[31] D.M. Stanković, M. Ognjanović, M. Fabián, V.V. Avdin, D.D. Manojlović, S. Vranješ.Đurić, B.B. Petković, CeO_2-doped – domestic carbon material decorated with MWCNT as an efficient green sensing platform for electrooxidation of dopamine, Surf. Interfaces 25 (2021) 101211, https://doi.org/10.1016/j.surfin.2021.101211.
[32] B.B. Petković, M. Ognjanović, B. Antić, V. Viktorovich Avdin, D.D. Manojlović, S. Vranješ Đurić, D.M. Stanković, Easily prepared Co_3O_4 doped porous carbon material decorated with single-wall carbon nanotubes applied in voltammetric sensing of antioxidant α-lipoic acid, Electroanalysis 33 (2021) 446–454, https://doi.org/10.1002/elan.202060290.
[33] B.B. Petković, M. Kostić, S. Samaržija-Jovanović, A. Ivanović, B. Laban, D. Veljović, D.M. Stanković, An efficient electrochemical sensing of caffeic acid at thermolysis

prepared urea-formaldehyde resin modified with Fe(III) and Ti(IV) oxide particles, Int. J. Electrochem. Sci. 17 (2022) 221214, https://doi.org/10.20964/2022.12.04.
[34] S. Đurđić, V. Stanković, D.M. Stanković, Graphitic carbon nitride in biosensing application, in: U.P. Azad, P. Chandra (Eds.), Handbook of Nanobioelectrochemistry, Springer Nature Singapore, Singapore, 2023, pp. 153–174, https://doi.org/10.1007/978-981-19-9437-1_8.
[35] J. He, Y. Xu, W. Wang, B. Hu, Z. Wang, X. Yang, Y. Wang, L. Yang, Ce(III) nanocomposites by partial thermal decomposition of Ce-MOF for effective phosphate adsorption in a wide pH range, Chem. Eng. J. 379 (2020) 122431, https://doi.org/10.1016/j.cej.2019.122431.
[36] D.A. Shirley, High-resolution X-ray photoemission spectrum of the valence bands of gold, Phys. Rev. B 5 (1972) 4709–4714, https://doi.org/10.1103/PhysRevB.5.4709.
[37] J.H. Scofield, Theoretical photoionization cross sections from 1 to 1500 keV., 1973. https://doi.org/10.2172/4545040.
[38] P. Shanmugam, G.P. Kuppuswamy, K. Pushparaj, B. Arumugam, A. Sundaramurthy, Y. Sivalingam, CeO_2 nanoparticles based extended gate field effect transistor for enzyme free detection of glucose, J. Mater. Sci. Mater. Electron 33 (2022) 9483–9489, https://doi.org/10.1007/s10854-021-07441-w.
[39] W.M. Ahmed Malik, S. Afaq, A. Mahmood, L. Niu, M. Yousaf Ur Rehman, M. Ibrahim, A. Mohyuddin, A.M. Qureshi, M.N. Ashiq, A.H. Chughtai, A facile synthesis of CeO_2 from the GO@Ce-MOF precursor and its efficient performance in the oxygen evolution reaction, Front. Chem. 10 (2022) 996560, https://doi.org/10.3389/fchem.2022.996560.
[40] K.I. Maslakov, Y.A. Teterin, A.J. Popel, A.Yu Teterin, K.E. Ivanov, S.N. Kalmykov, V.G. Petrov, P.K. Petrov, I. Farnan, XPS study of ion irradiated and unirradiated CeO_2 bulk and thin film samples, Appl. Surf. Sci. 448 (2018) 154–162, https://doi.org/10.1016/j.apsusc.2018.04.077.
[41] V. Matolín, M. Cabala, V. Cháb, I. Matolínová, K.C. Prince, M. Škoda, F. Šutara, T. Skála, K. Veltruská, A resonant photoelectron spectroscopy study of $Sn(O_x)$ doped CeO_2 catalysts, Surf. Interface Anal. 40 (2008) 225–230, https://doi.org/10.1002/sia.2625.
[42] S. Ansari, M.S. Ansari, H. Devnani, S.P. Satsangee, R. Jain, CeO_2/g-C_3N_4 nanocomposite: a perspective for electrochemical sensing of anti-depressant drug, Sens. Actuators B: Chem. 273 (2018) 1226–1236, https://doi.org/10.1016/j.snb.2018.06.036.
[43] M.C. Sekhar, N.S. Kumar, M. Asif, S.V.P. Vattikuti, J. Shim, Enhancing electrochemical performance with g-C_3N_4/CeO_2 binary electrode material, Molecules 28 (2023) 2489, https://doi.org/10.3390/molecules28062489.
[44] H.A. Abdu, D. Isabel, A.T. Abebaw, T.M. Abi, Polyaniline supported g-C_3N_4/CeO_2 fluorescent chemosensor for selected heavy metal and nitrate ions determination, Achi 30 (2022) 45–88, https://doi.org/10.47743/achi-2022-1-0003.
[45] L. Zhang, Z. Jin, S. Huang, Y. Zhang, M. Zhang, Y.-J. Zeng, S. Ruan, Ce-doped graphitic carbon nitride derived from metal organic frameworks as a visible light-responsive photocatalyst for H2 production, Nanomaterials 9 (2019) 1539, https://doi.org/10.3390/nano9111539.
[46] J. Wang, Electroanalytical techniques in clinical chemistry and laboratory medicine, VCH, New York, 1988.
[47] M.A. Hussein, A. Khan, K.A. Alamry, A highly efficient electrochemical sensor containing polyaniline/cerium oxide nanocomposites for hydrogen peroxide detection, RSC Adv. 12 (2022) 31506–31517, https://doi.org/10.1039/D2RA05041B.
[48] D.S. Grebenkov, Diffusion-controlled reactions: an overview, Molecules 28 (2023) 7570, https://doi.org/10.3390/molecules28227570.
[49] T.I. Abdullin, I.I. Nikitina, O.V. Bondar, Adsorption and oxidation of purine bases and their derivatives on electrodes modified with carbon nanotubes, Russ. J. Electrochem 44 (2008) 1345–1349, https://doi.org/10.1134/S1023193508120069.
[50] A.M. Oliveira-Brett, V. Diculescu, J.A.P. Piedade, Electrochemical oxidation mechanism of guanine and adenine using a glassy carbon microelectrode, Bioelectrochemistry 55 (2002) 61–62, https://doi.org/10.1016/S1567-5394(01)00147-5.
[51] R.N. Goyal, G. Dryhurst, Redox chemistry of guanine and 8-oxyguanine and a comparison of the peroxidase-catalyzed and electrochemical oxidation of 8-oxyguanine, J. Electroanal. Chem. Interfacial Electrochem. 135 (1982) 75–91, https://doi.org/10.1016/0022-0728(82)90006-7.
[52] Q. Li, C. Batchelor-McAuley, R.G. Compton, Electrochemical oxidation of guanine: electrode reaction mechanism and tailoring carbon electrode surfaces to switch between adsorptive and diffusional responses, J. Phys. Chem. B 114 (2010) 7423–7428, https://doi.org/10.1021/jp1021196.
[53] J. Martínez Guerra, A. Rojas-Hernández, D.S. Guzmán-Hernández, M.E. Palomar-Pardave, M. Romero-Romo, M.T. Ramirez-Silva, Electrochemical quantification of guanine in an aqueous medium using a bare carbon paste electrode, ECS Trans. 110 (2023) 199–205, https://doi.org/10.1149/11001.0199ecst.